Transient Response of Rotor on Rolling Element Bearings with Clearance

David P. Fleming
NASA Glenn Research Center
Cleveland, OH 44135, USA
David.P.Fleming@nasa.gov

Brian T. Murphy
RMA, Inc.
7701 Baja Cove
Austin, TX 78759, USA
bmurphy@xlrotor.com

Jerzy T. Sawicki
Cleveland State University
Cleveland, OH 44115, USA.
j.sawicki@csuohio.edu

J. V. Poplawski
J. V. Poplawski and Associates
Bethlehem, PA 18018, USA
Jvpoplawski@aol.com

ABSTRACT

Internal clearance in rolling element bearings is usually present to allow for radial and axial growth of the rotor-bearing system and to accommodate bearing fit-up. The presence of this clearance also introduces a "dead band" into the load-deflection behavior of the bearing. Previous studies demonstrated that the presence of dead band clearance might have a significant effect on synchronous rotor response. In this work, the authors investigate transient response of a rotor supported on rolling element bearings with internal clearance. In addition, the stiffness of the bearings varies nonlinearly with bearing deflection and with speed. Bearing properties were accurately calculated with a state of the art rolling bearing analysis code. The subsequent rotordynamics analysis shows that for rapid acceleration rates the maximum response amplitude may be less than predicted by steady-state analysis. The presence of clearance may shift the critical speed location to lower speed values. The rotor vibration response exhibits subharmonic components which are more prominent with bearing clearance.

KEY WORDS

Bearing clearance, Transient response, Rotordynamics, Rolling-element bearing stiffness, Dynamic analysis, Speed ramp analysis.

1. INTRODUCTION

Response of all but very flexible rotors depends strongly on bearing properties. When bearings are nonlinear, accurate rotor response calculations require use of bearing properties for the precise conditions encountered, rather than average properties. While fluid film bearings are often reasonably linear for small deflections (although there is usually a strong speed dependence), rolling-element bearings have a much less linear force-displacement relationship. Two aspects of rolling element bearings contribute further to nonlinearity. First, the bearings are often fabricated with internal clearance, or deadband. For example, in a 25 mm bore deep-groove ball bearing, the internal radial clearance (IRC) is typically between 4 and 13 μm. (For rotordynamic purposes it is most convenient to use bearing *radial* clearance as is done herein. However, bearing engineers more typically use internal *diametral* clearance (IDC), which is twice the internal radial clearance). Second, at speed, centrifugal forces move the rolling elements outward, increasing the clearance between the inner race and the rolling elements.

In previous papers [3, 4], the authors studied both steady-state and transient vibratory behavior as a rotor accelerated through a critical speed. They found that bearing nonlinearity strongly affected the rotor behavior, and furthermore that angular acceleration rate affected the maximum vibration amplitude at critical speeds. In these works, however, bearing deadband was not explicitly considered. Other authors have studied effects of

deadband. Tiwari et al. [7] considered the case of a balanced horizontal rotor with variable stiffness due to the changing position of the bearing balls as the shaft rotates. Childs [1] studied the effect of elliptical bearing clearances which produced vibration with a frequency of twice the rotational frequency (2/rev).

The present paper, as a sequel to [4], examines the effect of bearing deadband as a rotor accelerates through a critical speed. Accurate load- and speed-dependent bearing properties from the bearing code COBRA-AHS [5] are used. Response is calculated for the same rotor-bearing system as [4] for various rates of angular acceleration and various values of deadband.

The rotordynamic software XLRotor [6] was used to perform all numerical integrations. XLRotor was selected because it enables the use of user-defined routines for nonlinear elements. For this study, a Microsoft Excel Visual Basic Macro was written which computes the bearing reaction force as a function of both speed and deflection via a curve fit of the COBRA data (see below for more detail about this). For transient analysis, XLRotor provides several different numerical integration schemes, all of which are implicit and unconditionally stable. These types of integration schemes permit efficient integration of the full unreduced system of differential equations.

2. ANALYTICAL SYSTEM AND PROCEDURE

Figure 1 is a drawing of the shaft system. It depicts a fairly stiff shaft with concentrated masses (which may represent compressor or turbine wheels) at stations 5 and 7. In total, 11 stations and 10 elements were used in the model. Radial (deep groove) ball bearings of 25 mm bore diameter are at stations 2 and 10. The shaft material is steel; total mass of the shaft system is 4.6 kg.

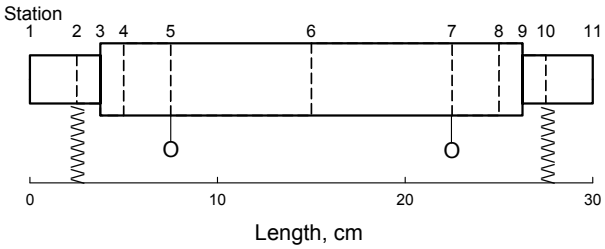

Figure 1: Sketch of rotor

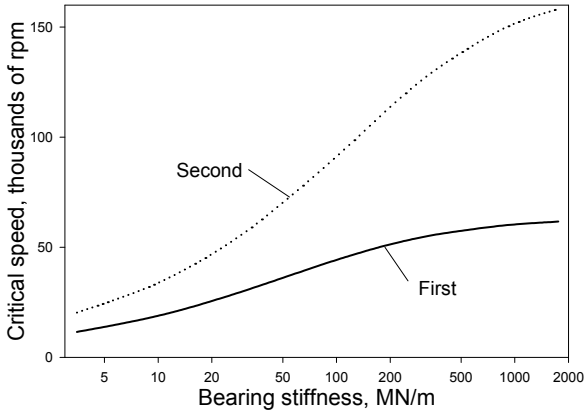

Figure 2: Critical speed map

Figure 2 shows the first two system critical speeds as a function of bearing stiffness. For stiffness up to about 200 MN/m, critical speeds rise rapidly with stiffness, indicating significant bearing participation in the rotor motion. Above 200 MN/m, critical speeds do not increase as rapidly, indicating that increasing amounts of motion are due to shaft bending rather than bearing deflection. Mode shapes calculated at critical speeds, presented in [3], confirm this.

COBRA-AHS was used to generate load versus deflection data for the bearings at speeds to 80 000 rpm and loads from near zero to 8800 N. COBRA computes deflection for a given load. At zero speed and near-zero load, the deflection equals the internal radial clearance (IRC). At elevated speed, the internal clearance opens up due to centrifugal loading of the balls against the outer race. So for any combination of speed and load, the deflection will be equal to the zero-load deflection plus additional deflection due to the load. This aspect is illustrated in the curves in Figure 3, where the increased deflection at 80 000 rpm compared to that at 10 000 rpm for the same load is apparent.

The method used to curve fit the COBRA data for each case of internal clearance was to first fit the data for zero-load clearance versus speed with a cubic polynomial.

$$x_0 = c_0 + c_1 N + c_2 N^2 + c_3 N^3 \tag{1}$$

where x_0 is the zero-load clearance, c_i are fitted coefficients, and N the speed. The zero load clearance was subtracted from all deflection values, essentially "normalizing" the deflection data to be zero at zero load. The

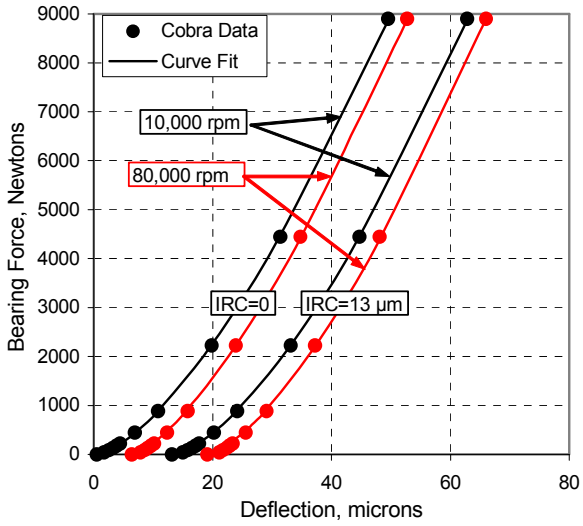

Figure 3: Load vs deflection for ball bearing.

entire matrix of normalized load/deflection/speed values was then fitted with the following formula, which is a simple power law with coefficient and exponent both linear in speed.

$$F = (k_0 + k_1 N)(x - x_0)^{(a_0 + a_1 N)} \qquad (2)$$

In equation (2), F is the bearing force, x the radial deflection, and the k and a are fitted coefficients. To subsequently compute the load for a given speed and deflection, equation 1 is used to compute the zero load clearance x_0. If the deflection is less than this value, the load is zero. If the deflection exceeds this, then equation (2) is used to compute the load. The coefficients fitted to equations (1) and (2) are shown in the Appendix, along with dimensions and other properties of the rotor model. Figure 3 illustrates that the curve fit does a good job of passing through the data points. The fitted curves are also smooth in both deflection and speed, which is highly desirable to prevent introduction of perturbations during transient analysis. The significant nonlinearity of the ball bearing is apparent. This figure also illustrates the significant clearance produced as a result of high speed operation.

The imbalance of 1.2 g-cm used in [4] was too small to produce a vibratory response when the bearings had internal clearance; the resulting center of gravity eccentricity was less than any bearing clearance considered. A larger imbalance of 3.6 g-cm, applied at station 7, was thus used for the present results. This produces an overall cg eccentricity of approximately 8 µm, which may be compared with the typical internal radial clearance of 4 to 13 µm. Thus the cg eccentricity still is less than the maximum bearing clearance one might expect in practice.

For the transient rotordynamic analysis, a constant time step of 10 microseconds was used for the 0.01, 0.05, and 0.25 second speed ramp cases. For the 1 second ramp cases, a time step of 7.8125 microseconds was used because it generated a more convenient number of output points. The number of time steps ranged from 1000, for the 0.01 second ramps, to 128,000 for the 1 second ramps. The numerical integration method employed was the generalized-α method with a controlling integration parameter of ρ_∞=0.8 [2]. The initial conditions were essentially zero for all cases starting from 10,000 rpm. For the deceleration cases starting from 80,000 rpm, the initial conditions were steady state response to imbalance at 80,000 rpm. By use of a short Microsoft Excel Visual Basic macro, the XLRotor software could run 12 combinations of ramp time and internal clearance in one unattended operation requiring a total of about 80 minutes on a Pentium class computer.

3. RESULTS

In previous work [4] with the rotor system used herein, the authors found that the shaft vibration amplitude at station 10, the bearing nearest the imbalance (applied at station 7) was a good measure of overall system vibration. While the response at station 7 was often greater than at station 10, due to the rotor mode shape, the responses at these stations tended to change together. Similarly, even with bearing nonlinearity, the overall appearance of a bearing load plot is quite similar to the appearance of station 10 amplitude. Therefore, results below are all presented as the motion at station 10. In addition, references [3] and [4] demonstrated that it is necessary to consider the nonlinear stiffness of rolling-element bearings in order to obtain accurate rotor response. Thus only results utilizing the accurate nonlinear bearing calculations will be presented herein; no calculations were made with linear bearings.

Vertical rotor acceleration from 10 000 to 80 000 rpm

Figures 4, 5, and 6 show the response over a speed range from 10 000 rpm to 80 000 rpm for three values of internal radial clearance and four acceleration rates with the rotor axis vertical (i.e., no gravity load on the bearings). In the keys of these and subsequent figures, the number before the underscore indicates the bearing IRC in microns, while the number after the underscore denotes speed ramp time in seconds. Initial amplitude of zero was assumed at the start of the calculations. Figure 4, for zero clearance, is similar to the data presented in [4]. Amplitudes are higher because of the larger imbalance used in the present study, and there are also minor differences due to the speed-dependent bearing data now employed. The longest acceleration time, 1 second, yields results very close to steady state in overall appearance until the critical speed is reached at 54,000 rpm.

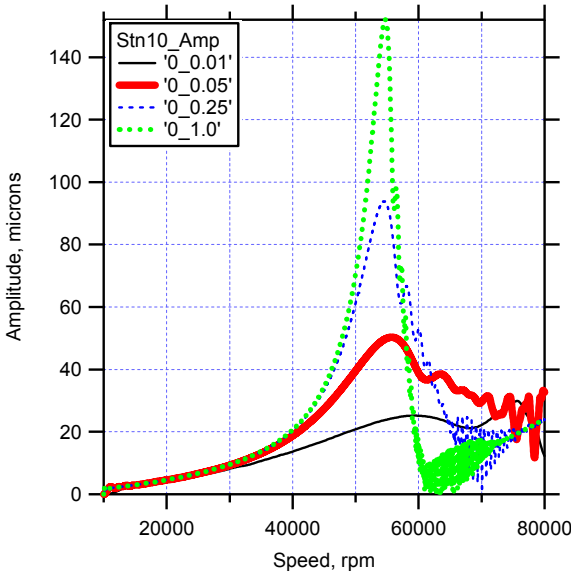

Figure 4: Speed ramp data with zero IRC.

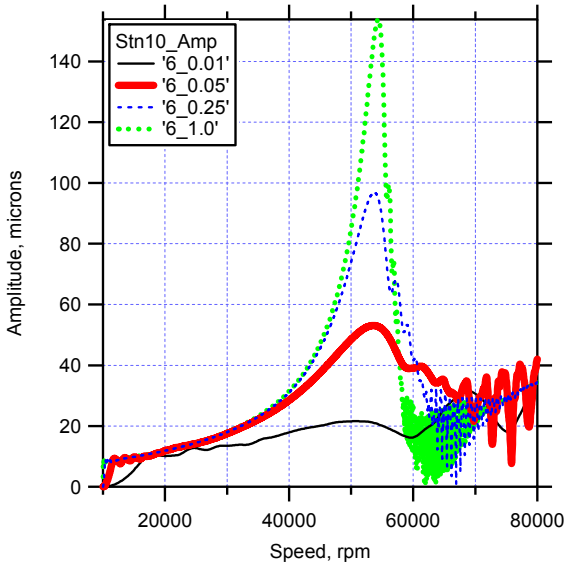

Figure 5: Speed ramp data for 6 μm IRC.

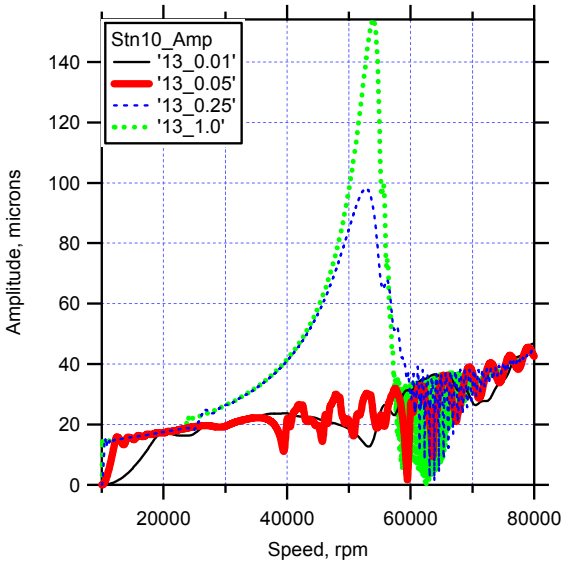

Figure 6: Speed ramp data for 13 μm IRC.

Above the critical speed, subharmonic oscillation appears; as discussed in [4], the frequency of this oscillation is approximately the rotor natural frequency at the low bearing stiffness corresponding to the low amplitudes of the supercritical region. Progressively shorter acceleration times lower the critical speed amplitude. Figures 5 and 6, for 6 and 13 μm IRC, respectively, are similar in appearance overall. Two differences are that the amplitude jumps up rather quickly to the corresponding bearing clearance as the speed rises (the initial amplitude was taken as zero), and also that the subharmonic oscillation in the supercritical region has a larger amplitude.

Each of figures 7 – 10 compares data for the same acceleration ramp time at different bearing clearances. Figure 7, for the slowest acceleration time of 1 sec., shows that the amplitude in the subcritical region is higher for larger clearance, as expected. The maximum amplitude is reached at nearly the same speed for all clearances. The three curves depicted are quite close together in the supercritical region out to about 60 000 rpm; above that speed larger clearance produces larger amplitude.

For a more rapid acceleration, 0.25 sec. from 10 000 to 80 000 rpm (fig. 8), overall amplitudes are lower than for the 1 sec case (note the different scales in the figures). Amplitudes are somewhat farther apart in the subcritical region, and the maximum amplitude occurs at a lower speed for larger clearances; at supercritical speeds a larger clearance results in somewhat lower amplitude out to about 65 000 rpm, but higher thereafter. The subharmonic oscillation is larger in magnitude at high clearance, and persists over a somewhat larger speed range.

For still more rapid acceleration, 0.05 sec. ramp time, figure 9, the curves for zero and 6 μm IRC appear as those for lower acceleration, but the amplitude for the 13 μm case does not pass through a conventional critical speed; subharmonic oscillation is prominent over most of the speed range.

At the highest acceleration investigated, 0.01 sec. ramp time (fig. 10), no obvious critical speed is evident for any bearing clearance.

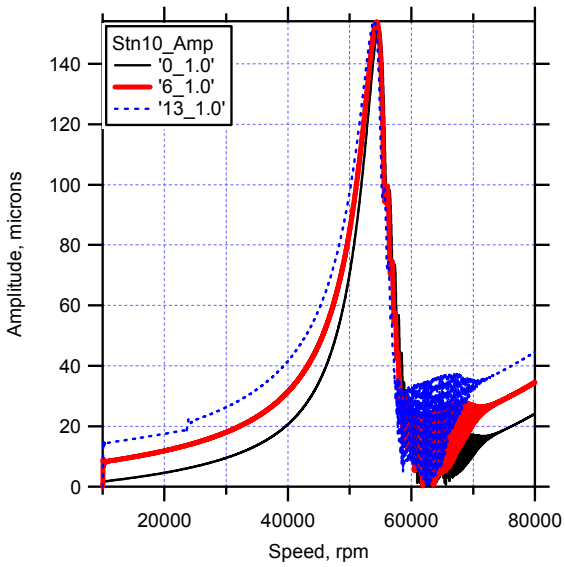

Figure 7: Acceleration data for 1 sec. speed ramp.

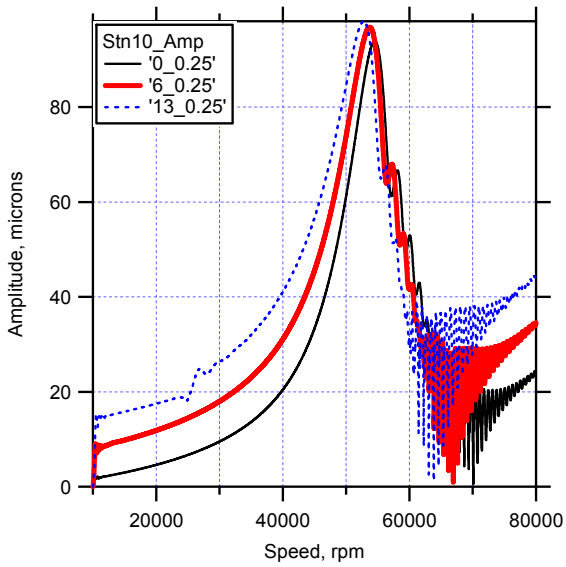

Figure 8: Acceleration data for 0.25 sec. speed ramp.

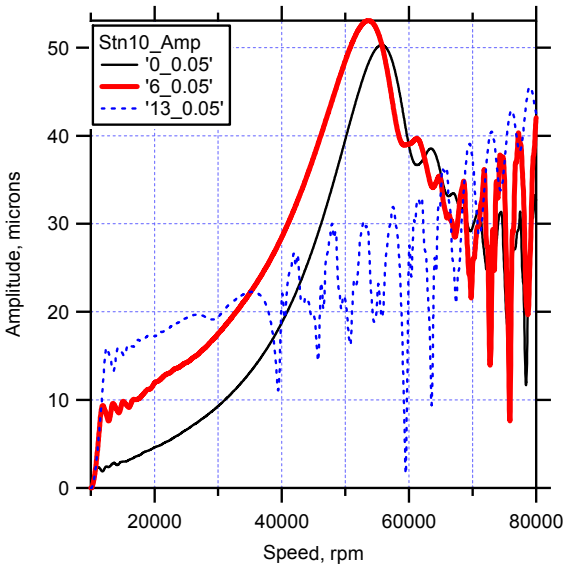

Figure 9: Acceleration data for 0.05 sec. speed ramp.

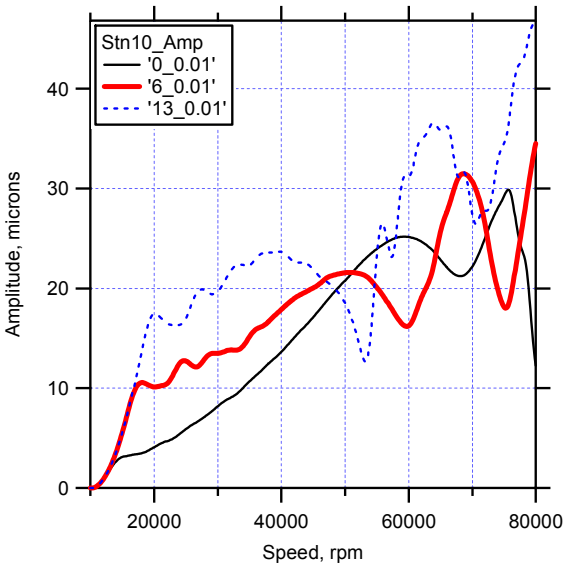

Figure 10: Acceleration data for 0.01 sec. speed ramp.

Vertical rotor deceleration from 80 000 to 10 000 rpm

As demonstrated in [3], with nonlinear bearings the amplitude – speed curves are different depending on whether the rotor is accelerating or decelerating. Using the steady-state case as an illustration, with a hardening bearing (which a ball bearing is), during acceleration the amplitude rises gradually to a peak and then suddenly jumps down to a low value in the supercritical region. During deceleration, the amplitude remains low until it suddenly jumps up.

Rotor deceleration curves are shown in figures 11 and 12. The initial conditions for the deceleration runs were the steady state conditions at 80 000 rpm. Figure 11, for 1 sec ramp time, corresponds to figure 7 for acceleration. It shows that amplitude generally drops as speed decreases until the speed is under where the maximum amplitude occurs on acceleration. Amplitude then jumps up as the rotor suddenly assumes subcritical operation. Superimposed on the motion are subharmonic oscillations, which extend over a larger speed range than during acceleration, although the subharmonic amplitudes are similar (again, the scales of the figures differ). The jump up occurs at lower speeds for larger bearing clearance. Figure 12, for 0.05 sec ramp time (compare with figure 9 for acceleration), does not show a definite jump, and the only case having a discernable critical speed is for zero clearance. Subharmonic oscillation is prominent over most of the speed range.

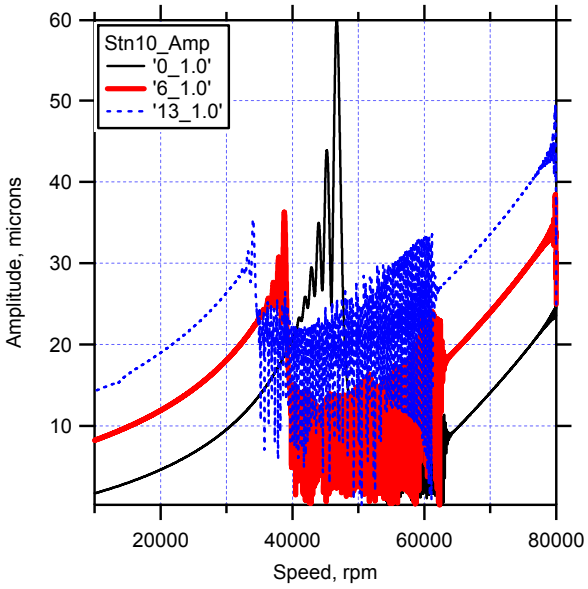

Figure 11: Deceleration data for 1 sec. ramp time.

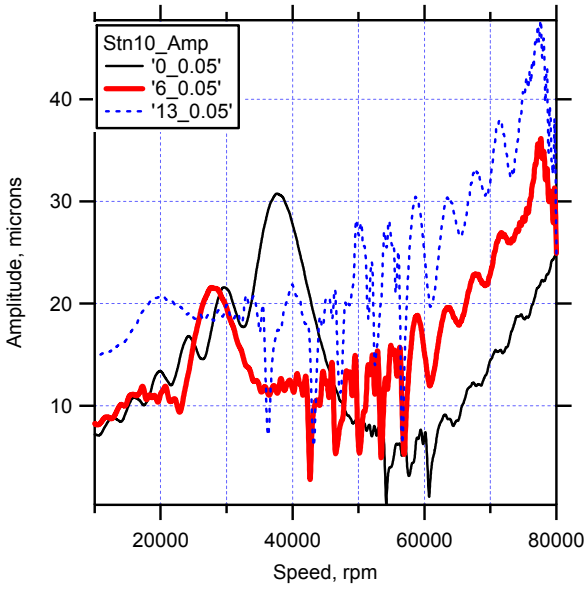

Figure 12: Deceleration data for 0.05 sec. ramp time.

Horizontal rotor acceleration from 10 000 to 80 000 rpm

When the rotor axis is horizontal, gravity applies a force which pushes the rotor toward the bottom of the bearings. When this force is greater than or comparable to the unbalance force, one would expect an effect on the rotor vibration. In actuality, the data appear little different from those for a vertical rotor with one exception. For the case of 13 μm IRC and a ramp time of 0.05 second, the curve for the horizontal rotor is much smoother up to the critical speed, as shown in figure 13 (compare with figure 9 for a vertical rotor). Above the critical speed, the subharmonic oscillations are somewhat more prominent for the horizontal case. It is at this clearance one would expect to see a difference, since the cg eccentricity is lower than the bearing clearance and the bearing does not necessarily make contact when there is no gravity load. But it is unknown at this point why the behavior at both shorter and longer ramp times is undifferentiated by gravity.

4. CONCLUSIONS

The behavior of an accelerating rotor supported by ball bearings having a clearance has been investigated. Overall, the behaviour was not markedly different because of clearance. As expected, rotor vibration amplitudes were higher with clearance in the subcritical region, but similar in the supercritical region. The subharmonic oscillations that were seen previously in the supercritical region were somewhat more prominent when the bearings had clearance. For a decelerating rotor, the subharmonic oscillations appeared over a larger part of the speed range than during acceleration. Adding a gravity load made little difference except for one speed ramp time when the rotor cg eccentricity was less than the bearing clearance.

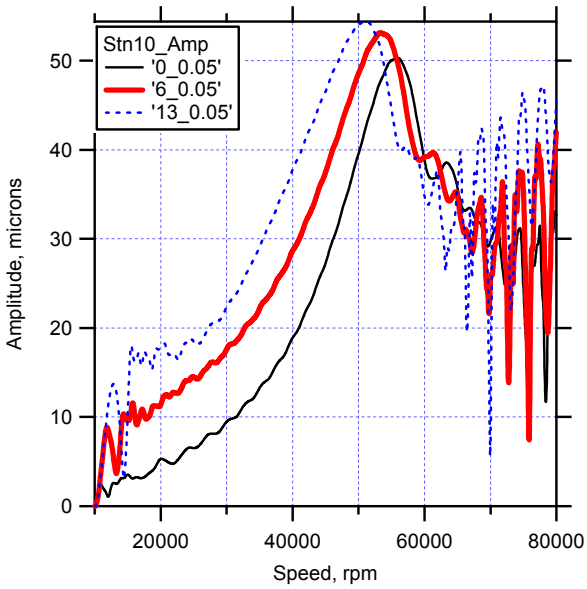

Figure 13: Acceleration data for horizontal rotor; ramp time, 0.05 sec.

REFERENCES

[1] Childs, Dara W. (2003): Twice-Running Speed Response Due to Elliptical Bearing Clearances. *J. Vibration and Acoustics, Trans. ASME*, vol. 125, pp. 64-67.

[2] Chung, J., and Hulbert, G. M. (1993): A Time Integration Algorithm for Structural Dynamics With Improved Numerical Dissipation: The Generalized-α Method. Journal of Applied Mechanics, vol. 60, pp 371-375.

[3] Fleming, D. P., and Poplawski, J. V. (2005): Unbalance Response Prediction for Rotors on Ball Bearings Using Speed and Load Dependent Nonlinear Bearing Stiffness. *International J. Rotating Machinery,* Vol. 2005, Issue 1, pp. 53-59 (online at www.hindawi.com/journals/ijrm/).

[4] Fleming, D. P.; Sawicki, J. T.; and Poplawski, J. V. (2005): Unbalance Response Prediction for Accelerating Rotors on Ball Bearings with Load-Dependent Nonlinear Bearing Stiffness. Proceedings of Third International Symposium on Stability Control of Rotating Machinery (ISCORMA-3), J. T. Sawicki and A. Muszynska, eds., pp. 512-519.

[5] Poplawski, J. V.; Rumbarger, J. H.; Peters, S. M.; Flower, R.; and Galaitis, H. (2002): Advanced Analysis Package for High Speed Multi-Bearing Shaft Systems: COBRA-AHS. Final Report, NASA Contract NAS3-00018.

[6] Rotating Machinery Analysis. www.xlrotor.com

[7] Tiwari, M.; Gupta, K.; and Prakash, O. (2000): Effect of Radial Internal Clearance of a Ball Bearing on the Dynamics of a Balanced Horizontal Rotor. *J. Sound and Vibration*, vol. 238, no. 5, pp. 723-756.

APPENDIX – Model Properties and Curve Fit Coefficients

For those wishing to utilize the model employed herein, data are shown here to high precision, rather than the rounded values presented in the text.

Model properties

Element	Length [mm]	Diameter [mm]
1	25.40	25.40
2	12.70	25.40
3	19.05	38.10
4	19.05	38.10
5	76.20	38.10
6	76.20	38.10
7	19.05	38.10
8	19.05	38.10
9	12.70	25.40
10	25.40	25.40

Density = 7833.5 kg/m^3
Elastic Modulus = 206.8 GPa
Shear Modulus = 79.6 GPa
Added at nodes 5 and 7:
M = 1.134 kg
I_{polar} = .004834 kg-m^2
I_{trans} = .002417 kg-m^2

Curve fit for gap versus rpm.

Gap $x_0 = c_0 + c_1 N + c_2 N^2 + c_3 N^3$ (Eq. 1)

Curve Fit Coefficient	Internal Clearance, radial		
	0 μm	6.35 μm	12.7 μm
c_0	-7.73499E-07	2.50202E-04	5.00214E-04
c_1	2.13619E-09	1.54882E-09	1.58395E-09
c_2	1.21009E-14	2.93985E-14	2.75680E-14
c_3	8.32779E-21	-1.21517E-19	-1.00795E-19

Curve fit for radial load versus rpm and radial deflection

Load $F = \left(k_0 + k_1 N\right)\left(x - x_0\right)^{\left(a_0 + a_1 N\right)}$ (Eq. 2)

Curve Fit Coefficient	Internal Clearance, radial		
	0 µm	6.35 µm	12.7 µm
k_0	2.02090E+07	2.27477E+07	2.52966E+07
k_1	-5.95030E+01	-6.23057E+01	-6.68524E+01
a_0	1.47827E+00	1.49894E+00	1.51737E+00
a_1	-7.29926E-07	-6.95007E-07	-6.80640E-07

These coefficients are applicable to radial displacements (x, x_0) in inches, speed (N) in rpm, and load (F) in pounds.

During analysis the load is resolved into Cartesian coordinates, and a linear viscous damping force is added, due to instantaneous velocity, with a damping coefficient of 1800.2 N-s/m (10.28 lb-s/in).